Effect of PVD-coated chromium on the subcooled flow boiling performance of nuclear reactor cladding materials

Effect of PVD-coated chromium on the subcooled flow boiling performance of nuclear reactor cladding materials

Jee Hyun Seong, Chi Wang, Bren Phillips, Matteo Bucci[*]

Department of Nuclear Science and Engineering, Massachusetts Institute of Technology, Cambridge, MA 02139, USA

[*]Author to whom correspondence should be addressed: mbucci@mit.edu

Abstract

We elucidate the separate effect of a thin Cr coating deposited by physical vapor deposition (PVD) on the subcooled flow boiling performance of zircaloy-4. First, we run flow boiling experiments on prototypical zircaloy-4 surfaces mimicking the scratch pattern and surface roughness of nuclear reactor claddings. Then, we PVD-coat a 0.3 μm thick chromium layer on the same exact surface and repeat the same flow boiling investigations. All experiments are run using deionized water at atmospheric pressure, flowing on a 1×3 cm^2 rectangular cross section channel at a rate of 1000 $kg/m^2/s$ and a subcooling of 10 K. We measure the average temperature of the boiling surface at increasing surface heat fluxes, covering a wide range of heat transfer regimes, from single-phase forced convection to the boiling crisis. We also record high-speed videos of the boiling process, which we postprocess to measure bubble nucleation site density, growth time, departure diameter and frequency. The surface analysis reveals that, while the chromium coating does not seem change the surface roughness and morphology, it improves surface wettability. However, it decreases the critical heat flux. The chromium coating causes an increase of nucleation temperature, bubble departure diameter and growth time, and a reduction of the nucleation site density. The concurrence of these observations indicates that a size reduction of the nucleation sites, conformally covered by the chromium coating, may be the cause of the boiling performance deterioration. We confirm this hypothesis repeating the same analysis on a FeCrAl sample prepared and tested using the same protocol as the zircaloy-4 sample, but with a different initial surface texture.

Keywords: Boiling, Accident Tolerant Fuel, PVD, chromium, zircaloy-4, FeCrAl

1. Introduction

The fuel cladding is a key component of a nuclear reactor system. Light water reactor (LWR) fuel claddings are typically made of zircaloy, i.e., zirconium alloys. Zirconium alloys are attractive because of their favorable neutronic properties and high melting point temperature. However, they may experience severe oxidation and generate hydrogen (produced by the oxidation reaction itself) when exposed to high temperature steam. This is not the case in normal operating conditions. However, it might happen during an unlikely loss of coolant event, e.g., after the tsunami that hit the Fukushima nuclear power plant in 2011. Since the early 2010, the nuclear community has focused on the development of accident tolerant fuel (ATF) cladding materials with enhanced resistance to oxidation and hydrogen generation [1-8]. As of today, chromium-coated zircaloy is one of the most promising concepts. Micrometric chromium coatings can enhance the oxidation resistance of zircaloy claddings (typically ~0.6 mm thick) without affecting their thermomechanical strength. However, these coatings may change the surface wettability and morphology, which are known to affect boiling heat transfer efficiency and critical heat flux (CHF). As CHF represents, among other things, a crucial operational limit for nuclear reactors, there is a scientific and technical interest in understanding how it may be affected by such chromium coatings.

Several studies have investigated the pool boiling performance of Cr-coated surfaces [9-15]. Chromium can be coated using different physical or chemical processes, e.g., physical vapor deposition (PVD), electroplating, and cold spray. PVD-coated chromium coatings are typically thin, i.e., their thickness is smaller or comparable to the characteristic length scale of the underlying surface features (e.g., the surface roughness R_a). Such coatings cover the surface conformally, i.e., they preserve, to some extent, the morphology of the underlying surface. Meanwhile, spray-coated chromium coatings are typically thick (i.e., they do not preserve the morphology of the underlying surface) and rough and are typically polished after the deposition. Importantly, these different processes lead to different surface textures and wettability [8, 16] and, consequently, a different boiling performance. Crucially, there is still no general agreement on how these coatings may affect the boiling heat transfer process. Table 1 summarizes recent experimental works investigating the boiling performance of chromium coatings. Kam et al. [9] and Jo et al. [13] observed that Cr coatings obtained by electroplating (1 µm thick) and cold spray (64 to 79 µm thick, polished after coating) reduce CHF and argued that such behavior is due to a deterioration

of the surface wettability. Lee et al. [16] also reported reduced CHF and enhanced heat transfer coefficient on a cold sprayed chromium coating in subcooled flow boiling, but they attributed those changes to a change of the surface morphology, leading to a decrease of the bubble departure diameter and an increase of the nucleation site density, rather than wettability. Son et al. [15] reported that a 1.5 μm thick chromium layer PVD-coated at room temperature makes the surface super-hydrophilic and enhances CHF. Conversely, subcooled flow boiling experiments conducted by Lee et al. [16] revealed no meaningful changes in heat transfer coefficient and CHF on PVD-coated surface with a slightly deteriorated surface wettability. In summary, while the understanding of these phenomena is improving, the number of variables to consider (e.g., the type of coating technique, sample surface finish, and the operating conditions) is large, and targeted studies are necessary to elucidate coating-specific effects.

In this regard, the objective of this work is to elucidate the separate effect of thin PVD-coated chromium coatings on the surface properties and the subcooled flow boiling performance of nuclear reactor cladding materials in low pressure conditions. Importantly, in a recent study on the separate effect of surface oxidation [17], we demonstrated that the subcooled flow boiling performance (i.e., heat transfer coefficient and CHF) of unoxidized zircaloy-4 surfaces can be different even on samples with the same nominal wettability and roughness, presumably due to random differences in the nucleation site size distribution. This result has profound implications, as it suggests that to elucidate the separate effect of thin coatings (e.g., PVD-coated chromium) preserving the morphology of the underlying surface, one should compare the boiling behavior of the same exact sample, before and after the PVD process. In this work, we conduct these separate effect investigations on two different samples, i.e., a zircaloy-4 sample with a scratch pattern and surface roughness comparable to a nuclear reactor cladding, and a FeCrAl sample, prepared using the same exact fabrication protocol, but presenting a different initial surface texture. Crucially, the experiments feature high-speed video diagnostics through which we can quantify the boiling parameters and understand how the coating change the boiling behavior.

Table 1. Summary of ATF boiling studies on Cr-coated surfaces

Author		Kam et al. [9]	Jo et al. [13]	Son et al. [15]	Lee et al. [16]	
Boiling condition		Pool boiling			Subcooled flow boiling	
Uncoated substrate	Material	SS	ZIRLO	SS	Zircaloy-4	
	Thickness (mm)	1.2	0.8	2	0.6	
	Contact angle (°)	61±5	64±3	63±5	81±3	
	Average roughness, R_a (nm)	25±2	120	111±22*	112	
	CHF (kW/m^2)	1020	645	700	2590±20	
Cr-coating	Coating technique	Electroplating	Cold spray	Sputtering**	Cold spray	Sputtering
	Coating thickness (μm)	1	64~79	1.5	(not specified)	(not specified)
	Contact angle (°)	81±4	77±6	0 (super-hydrophilic)	94±6	88±5
	Average roughness, R_a (nm)	27±1	74***	123±10	532	166
	CHF (kW/m^2)	660	571	1015	2290±20	2580±1I
Interpretation	Effect on CHF	Deteriorated	Deteriorated	Enhanced	Deteriorated	No change
	Determining factor	Wettability	Wettability	Wettability	Morphology	-

* Selected case polished with 800-grit sandpaper.
** Selected case sputtered at room temperature.
*** Polished with 600-grit sandpaper after deposition.

2. Experimental set-up and methods

We conduct our boiling experiments on 20 × 20 mm^2 monolithic metallic substrates with a nominal thickness of 1 mm [Fig. 1 (a)]. These substrates are made of zircaloy-4 or KANTHAL® APMT FeCrAl. One side of the substrate is in contact with air, whereas the other side is in contact with water. The substrate is heated using a thin film heater coated on the side of the substrate in contact with air, i.e., the air side. Heating elements and electrodes are sputtered to create a 10 mm × 10 mm active heating area. The heat released by Joule effect by the thin film heater is conducted through the substrate towards the boiling side. For more details about the composition and fabrication of these heating layers, we direct the reader to Ref. [17]. The heater is installed into a ceramic cartridge [Fig. 1 (b)], flushed with the walls of a vertical, 1 × 3 cm^2 rectangular cross-section flow channel. The cartridge is forerun by a long entrance region (more than 60 hydraulic diameters) to reach fully developed flow conditions at the height of the heater. For more details about the flow loop, we direct the reader to Ref. [18].

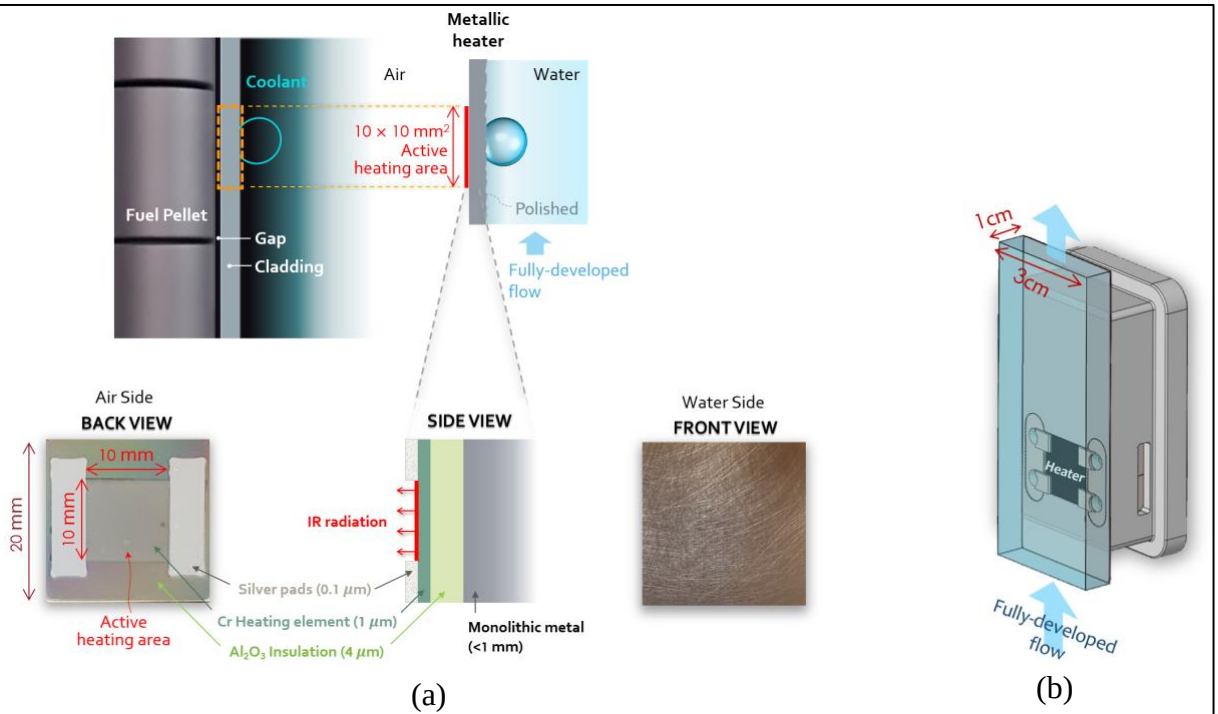

Fig. 1. Experimental set-up. (a) Metallic heater design [17]. (b) Heater cartridge and flow channel.

Fig. 2 shows the arrangement of the high-speed video and infrared diagnostics. The time dependent 2-D temperature distribution of the active heating area in contact with air is recorded by an IRC806HS infrared (IR) camera with a pixel resolution of 115 μm/pixel and a temporal

resolution of 2500 frames per second (fps). These temperature distributions are time-averaged and used as input of an inverse conduction model through which we can quantify the average temperature and heat flux on boiling surface [17]. The boiling process is also recorded in front-lit shadowgraphy by a Phantom® v2512 high-speed video (HSV) camera with a pixel resolution of 30 μm/pixel and a temporal resolution of 10000 fps.

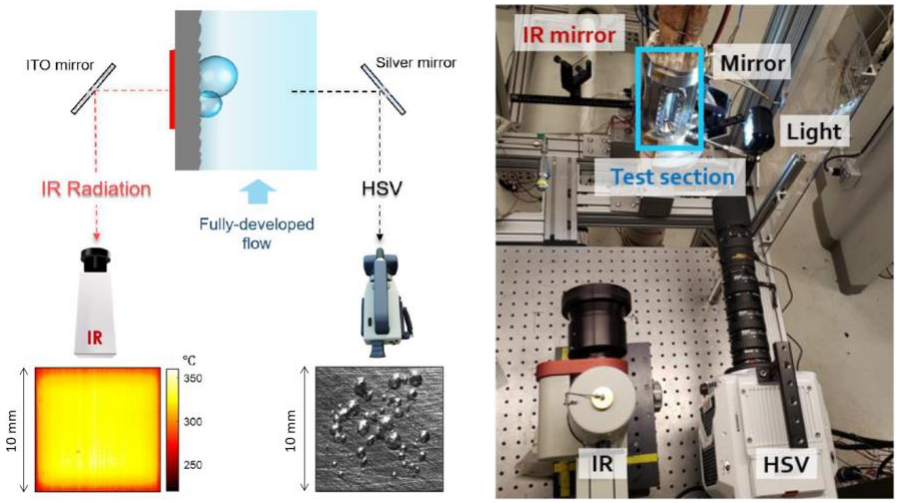

Fig. 2. Optical arrangement of the high-speed video and infrared diagnostics.

We engineer the boiling surface using the procedure developed in our previous study [17]. Briefly, as-received Zircaloy-4 and FeCrAl coupons are simultaneously and uni-directionally polished with a Buehler CarbiMet™ 240-grit sandpaper in order to achieve a scratch pattern and an average roughness comparable to commercial fuel claddings, i.e., 0.1~0.6 μm [19]. Finished samples are sonicated in Acetone and then rinsed with Ethanol, Isopropanol, and DI water to remove residual debris. After running subcooled flow boiling experiments, the boiling surfaces are thoroughly cleaned by Isopropanol and DI water. Then, we PVD-coat a 0.3μm-thick Cr coating on the boiling surface. To that end, we use a Kurt J. Lesker PRO PVD system at a deposition rate of 1Å/s, with a Kurt J. Lesker No. EJTCRXX352TK4 chromium target, powered by a 80 W DC gun. The system is operated with an Argon inert atmosphere at 3E-3 torr of working pressure. As mentioned, the procedure to create the thin film heater on the airside of the heater is detailed in Ref. [17]. The thin film heater is re-coated on the airside of the chromium coated sample since it can get damaged when the uncoated sample is removed from the cartridge, once the boiling experiment is complete.

3. Surface characterization

The micro- and nano-scale morphology images of the exact same region of a sample before and after Cr-coating are shown in Fig. 3. Fig. 3 also summarizes the values of average surface roughness, S_a, obtained from optical profilometer analyses, and roughness ratio, *r*, obtained through atomic force microscopy (AFM) analyses.

Polished Zircaloy-4 and FeCrAl samples prepared using the same fabrication protocol have comparable average surface roughness, but a rather different roughness ratio. The roughness ratio of the uncoated FeCrAl surface is twice the roughness ratio of the uncoated zircaloy-4 surface. We may speculate that this difference is due to the different hardness of the two materials. However, further analyses would be required to demonstrate this hypothesis. The chromium coating on Zircaloy-4 does not change average surface roughness nor roughness ratio, but it increases the surface wettability. Precisely, the contact angle (CA) decreases from $43^\circ \pm 2^\circ$ to $27^\circ \pm 3^\circ$ when the surface is coated. Instead, the chromium coating reduces significantly the roughness ratio of the FeCrAl surface, making it comparable to the roughness ratio of the zircaloy-4 surface (uncoated or coated). This is because the chromium coating is thick enough to cover and smooth out the rugged sub-micron surface features present on the FeCrAl surface (but not on the Zircaloy-4 surface), whereas it is thin enough not to smoothen the micron-scale structures of the surface (which are similar to those on the Zircaloy-4 surface). At the same time, the chromium coating also improves the surface wettability, making the contact angle to decrease from $68^\circ \pm 3^\circ$ to $28^\circ \pm 5^\circ$. In summary, the two chromium coated surfaces have very similar properties. Scanning electron microscopy (SEM) images reveal how the thin PVD-coated chromium modifies the surface texture. The 0.3 μm thick chromium coating is like a compact (i.e., non-porous) "snow" layer that coats conformally the larger features and clutters and smoothens out the smaller ones (note that the line profiles shown in the bottom figures are plotted compared to the average line profile values). These observations resonate with the findings of Umretiya et al. [8], who reported a slight increase of the average surface roughness and a decrease of the contact angle on surfaces PVD-coated with chromium. Their work also revealed that the coated surfaces have rounded-shape asperities and argued that rounded sub-micron features improve the surface wettability.

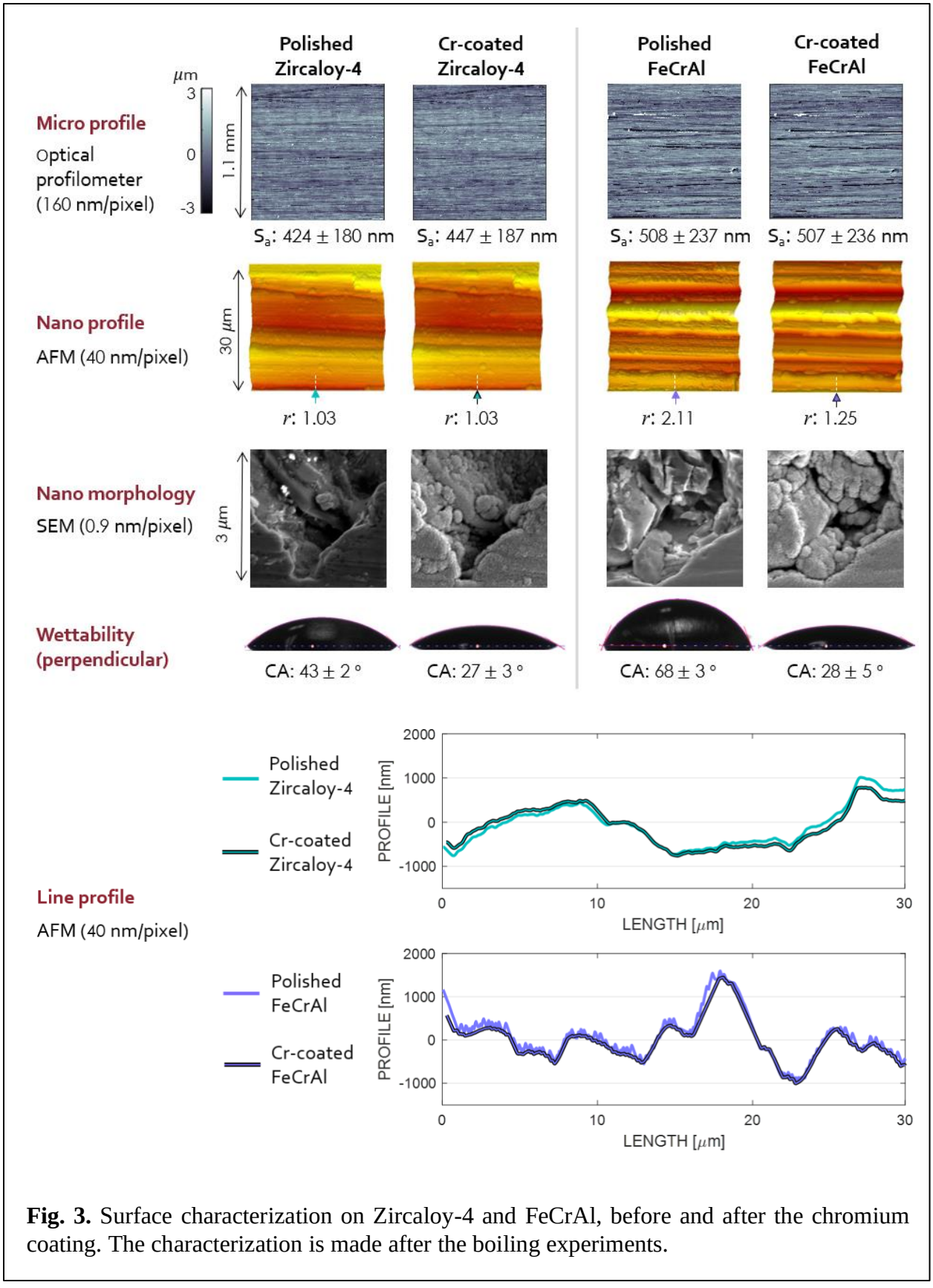

Fig. 3. Surface characterization on Zircaloy-4 and FeCrAl, before and after the chromium coating. The characterization is made after the boiling experiments.

1

4. Subcooled flow boiling results and discussion

We conduct all our experiments using deionized water at atmospheric pressure, flowing at a rate of 1000 kg/m^2/s and with a subcooling of 10 K. Before running boiling experiments, non-condensable gases in the flow loop are removed using a degassing filter at room temperature. For each surface, we increase the surface heat flux in steps of approximately 100 kW/m^2, covering a wide range of heat transfer regimes, from single-phase forced convection to the boiling crisis. At each heat flux step, we record high-speed infrared and front-lit shadowgraphy videos using the IR and HSV cameras, respectively. CHF is detected through a temperature spike in the airside of the heater, imaged by the infrared camera. When that happens, the electric power supply is immediately cut in such a way that the heater does not burn. We repeated the same experiment twice, but during the second run we limited the heat flux to 1500 kW/m^2. The results of the additional runs are shown in Appendix A, and confirm the results discussed hereafter.

The boiling curves of the Zircaloy-4 and FeCrAl samples, with and without the chromium coating are shown in Fig. 4. The shadowed area in a boiling curve represents mostly the standard deviation of the time-averaged spatial temperature distribution, which is much larger compared to other sources of uncertainties, e.g., measurements errors, ± 1℃ (see Ref. [17] for details of uncertainty analysis). Heater thickness, CHF value, average surface roughness, roughness ratio and contact angle are summarized in Table 2. One may note that the coated sample is thinner than the uncoated sample. That happens because after the boiling experiment on the uncoated sample we need to polish and re-coat the thin film heater on the airside of the sample, as mentioned in the previous section. However, we make sure that the heater thickness is always larger than the minimum asymptotic thickness below which the CHF is known to decrease when the heater thickness decreases, as reported in many references [20-29].

As shown in Fig. 4, the chromium coating, which improves the surface wettability, decreases both the heat transfer coefficient (i.e., the wall superheat required to remove the same heat flux from the boiling surface is higher) and the CHF limit, for both the zircaloy-4 and the FeCrAl sample. This finding is in contrast with the common sense, mostly based on pool boiling experiments, that improving the surface wettability increases the CHF limit. This work and our previous study on the separate effect of surface oxidation [17] seem to indicate that in flow boiling (at least in our operating conditions) wettability may be overshadowed by other effects and plays a secondary role. Instead, the dynamics and effectiveness of the boiling process are likely

determined by the size distribution of the bubble nucleation sites. This hypothesis is supported by the post-processing and analysis of the high-speed images presented hereafter.

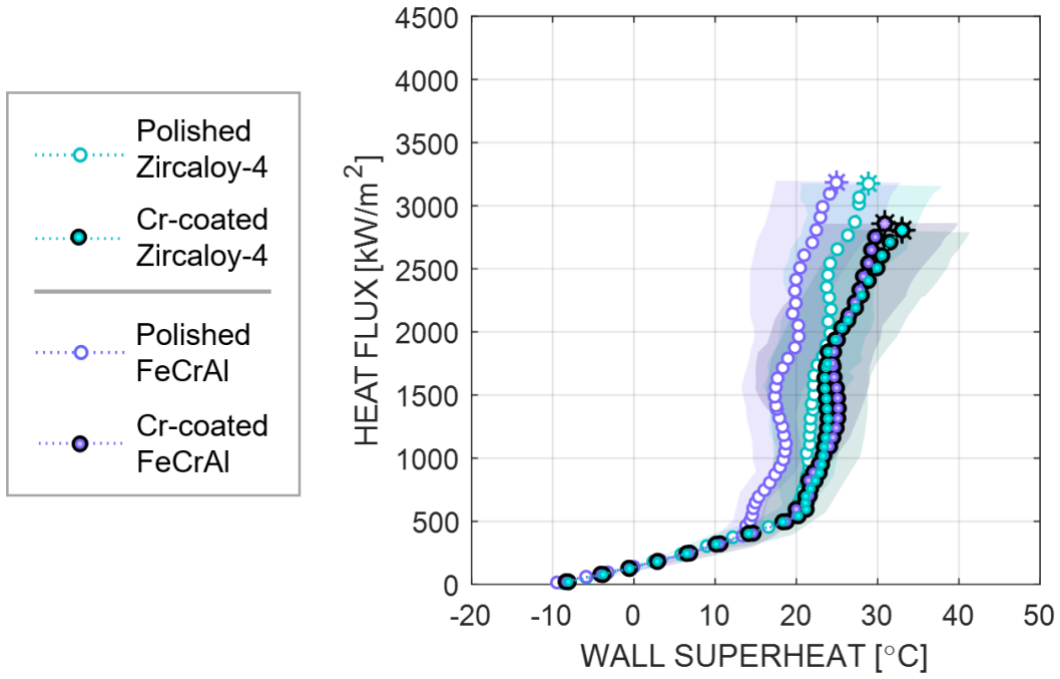

Fig. 4. Boiling curves of the Zircaloy-4 and FeCrAl before and after Cr-coating.

Table 2 Heater thickness, CHF value, and surface properties for the data given in Fig. 4.

	Polished Zircaloy-4	Cr-coated Zircaloy-4	Polished FeCrAl	Cr-coated FeCrAl
Thickness (mm, ±0.01)	0.98	0.8	0.92	0.79
CHF (kW/m^2,±10)	3175	2858	3184	2806
Average surface roughness (nm)	424±180	447±187	508±237	507±236
Roughness ratio	1.03	1.03	2.11	1.25
Contact angle (°)	43±2	27±3	68±3	28±5

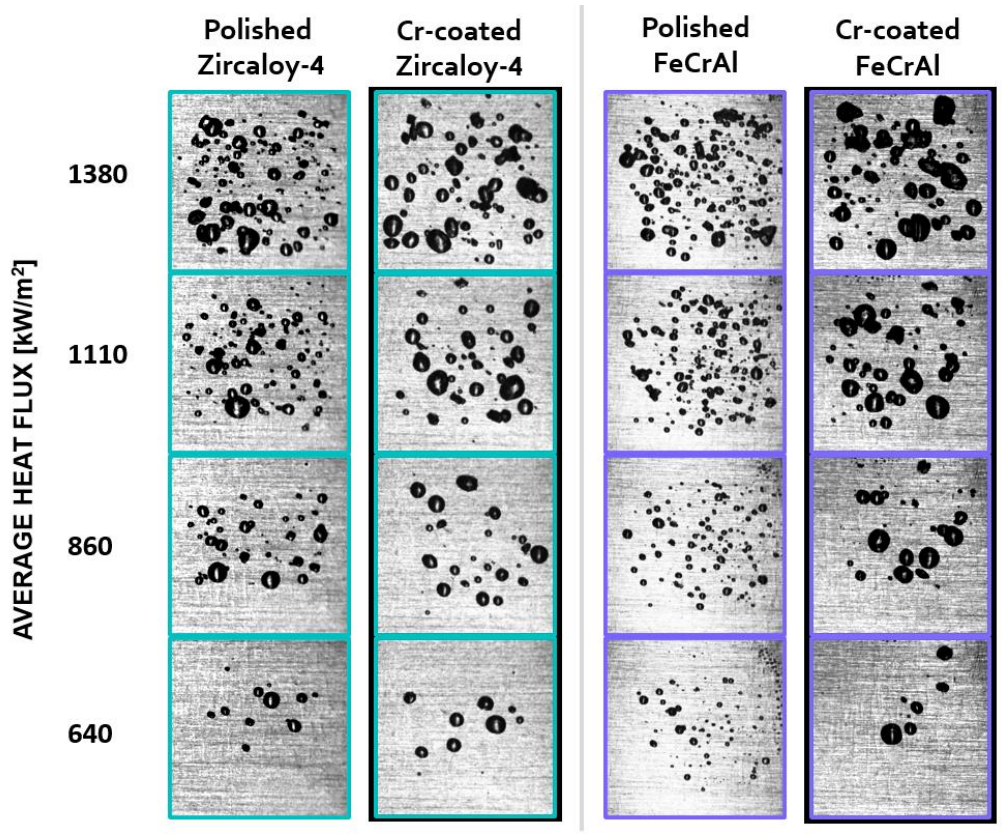

Fig. 5. HSV images for the data given in Fig. 4.

Qualitatively, Fig. 5 shows that, for the same heat flux conditions, the chromium coating decreases the number of bubbles and make them bigger. HSV images are post-processed using ad-hoc algorithms [30] developed in house. These post-processing algorithms use convolutional neural network [31] to segment the images and optical flow algorithm [32] to quantify the fundamental boiling parameters plotted in Figs. 6. Fig. 6 (a) throughout (d) show how measured departure diameter, growth time, nucleation site density and bubble departure frequency change with the heat flux for both uncoated and chromium-coated zircaloy-4 and FeCrAl samples. Note that the maximum heat flux in Fig. 6 is not the CHF. The high-speed video analysis is possible only at lower heat fluxes, for which the boiling surface is not obscured by bubbles, and the front-lit shadowgraphy imaging technique works properly.

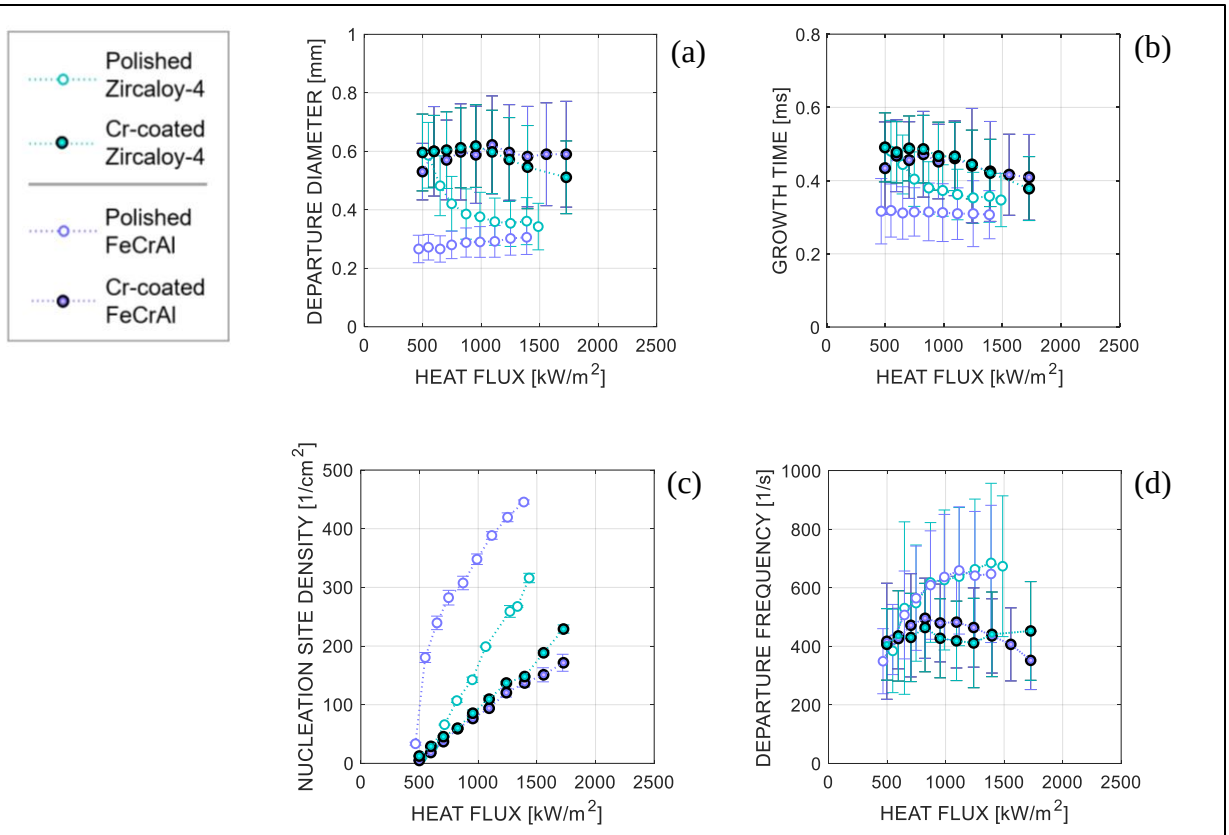

Fig. 6. Measured departure diameter (a), growth time (b), nucleation site density (c), and bubble departure frequency (d), at several heat fluxes, for both uncoated and chromium coated zircaloy-4 and FeCrAl samples.

Based on the boiling curves [Fig. 4], the onset of nucleate boiling (ONB) temperature on the uncoated and chromium coated zircaloy-4 surfaces are very similar, i.e., around 20 °C. Such wall superheat is consistent with a vapor-trapped cavity radius (predicted using Young-Laplace equation) of roughly 400 nm, which is in the order of magnitude of the surface average roughness. Also, bubble departure diameter, growth time, nucleation site density and departure frequency at the ONB conditions (i.e., the lowest heat flux values in Fig. 6) are very similar. However, as the heat flux increases, the coated and uncoated zircaloy-4 surfaces develop a different behavior [Fig. 6]. The coated surface has larger bubble departure diameter and growth time, and smaller bubble departure frequency and nucleation site density. The concurrence of these observations suggests that, while the average surface temperature is not much higher, bubbles may nucleate at higher temperature on the coated surface (unfortunately, this kind of experiments does not allow to measure the exact nucleation temperature at each nucleation site, but only the surface average

temperature). This hypothesis can also explain why, despite the coating-improved wettability should promote bubble detachment from the heated surface, their departure diameter is bigger compared to the uncoated surface [Fig. 6 (a)]. This effect could be explained through the inertia of the surrounding liquid, which hinders the bubble detachment from the surface [33]. In fact, the liquid inertia force is proportional to the bubble growth rate, and the bubble growth rate is (everything else being the same) proportional to the nucleation temperature. Precisely, classical models (e.g., see review in Ref. [34]) predict that the bubble growth rate, mostly limited by the thermal diffusion in the thermal boundary layer, is proportional to Jacob number, i.e., to the nucleation superheat. In these conditions, the liquid inertia force holding the bubble attached to the surface is also proportional to the nucleation superheat [35]. Thus, as these bubble-departure-impairing inertial effects may dominate over bubble-departure-promoting surface wettability effects, bubbles nucleating at higher temperature on the coated surface have to grow bigger (compared to the uncoated surfaces) before the lift and drag forces created by the liquid flow can make them detach from or slide over the surface. In summary, a higher nucleation temperature leads to larger bubbles and longer growth times [Fig. 6 (b)], as predicted by force balance models for flow boiling conditions [18, 35]. The energy removed by each bubble is, in a first order approximation, proportional to the bubble radius to the power two [36]. Consequently, larger bubbles remove more energy and create larger fluctuations of the spatio-temporal temperature distribution on the boiling surface. Unfortunately, as mentioned before, such kind of experiments do not allow to measure the exact nucleation temperature at the nucleation sites, nor the time-dependent distributions on the boiling surface. Thus, this reasoning is purely speculative. However, previous studies using high-resolution infrared thermometry seem to support this idea [36]. The increase of nucleation superheat also leads to longer wait times. Precisely, the wait time is expected to the be proportional to the nucleation superheat to the power two [18]. Overall, longer growth time and wait time result in a lower departure frequency [Fig. 6 (d)]. The presence of larger bubbles that take longer to detach from the boiling surface is compensated by a decrease of nucleation site density [Fig. 6 (c)], as also observed in previous studies using high-resolution infrared diagnostics to compare the behavior of rough and nano-smooth surfaces in the same flow boiling conditions [36]. However, while this description is consistent with the picture offered by Fig. 6, it still does not explain why the nucleation temperature should increase. It could be due to the surface wettability, as improving the wettability (i.e., reducing the contact angle) make the nucleation

condition more challenging to reach (i.e., it requires a higher wall superheat). However, classical models suggest that, as long as the contact angle is below 90˚, the nucleation temperature of vapor embryos trapped in the surface cavities should not change [34]. Also, and importantly, our recent study on the effect of zircloy-4 oxidation showed that the wettability enhancement due to surface oxidation with contact angles decreasing from 50˚ to 31˚ (i.e., in these same order of magnitude as ours) and without any alteration of the surface morphology, did not produce any change in boiling curve and CHF. These arguments seem to disprove the wettability effect and suggest that, instead, the reason for the increase of the nucleation temperature may be a reduction of the nucleation cavity size due to the chromium coating, as predicted by Hsu's nucleation bubble nucleation model [37]. SEM images of the boiling surface [Fig. 3] show that small cracks and crevices on the boiling surface (potentially serving as nucleation sites) gets cluttered by the coating, corroborating this hypothesis. Note that the ONB conditions (see Fig. 4) for the uncoated and coated surfaces are very similar. This suggests that the Cr-coating mostly affects cavities of smaller size (compared to ONB point), which nucleate at higher temperature.

The results of the tests performed on FeCrAl are consistent with conclusions drawn on the zircaloy-4 samples. On the uncoated FeCrAl surface, bubbles nucleate at lower temperatures compared to the uncoated zircaloy-4 surface. The ONB wall superheat is approximately 14 ℃. This value is consistent with a vapor-trapped cavity radius (predicted using Young-Laplace equation) of roughly 650 nm, which is not far from the order of magnitude of the surface average roughness. Bubbles are tiny when they depart from the heated surface. Their growth time is relatively short, and their departure frequency is high (i.e., the wait time, which is a large fraction of the bubble period, is also short compared to the other surfaces). This process results in a very high nucleation site density and overall, makes the boiling process very effective. Such boiling dynamics, consistent with the explanation provided before, is likely caused by the surface micro-texture. Interestingly, when the surface is PVD-coated with 0.3 μm of chromium, the concurrent smoothening of the surface texture and the enhanced wettability make the boiling process very similar to the one on the chromium coated zircaloy-4 sample. In passing, we emphasize that FeCrAl is another promising candidate ATF cladding material and that it does not require a chromium coating to enhance its resistance to oxidation in high temperature steam. In this context, we use FeCrAl because it has a different surface texture (compared to zircaloy-4 surfaces prepared

using the same fabrication procedure) exacerbating the influence of the chromium coating, and as such it offers the possibility to consolidate our findings and hypotheses. However, our results suggest that surface finish, and not the material itself, determines the boiling performance. The chromium coated surfaces have in fact a very similar boiling dynamics and CHF, no matter the substrate material. This statement may fall short if the materials thermal diffusity and diffusivity are very different, which is not the case for zircaloy-4 and FeCrAl, or even other materials of interests for the nuclear industry, e.g., Inconel (see Fig.9 in the Appendix B).

5. Conclusions

We studied the separate effect of thin PVD-coated chromium coatings on the subcooled flow boiling performance of rough zircaloy-4 surfaces mimicking the scratch pattern and roughness of nuclear reactor fuel claddings. We also consolidated our findings and hypotheses probing the effect of these coatings on FeCrAl surfaces, with a different uncoated surface texture.

Our results show that, while the chromium coating improves the surface wettability, it decreases the CHF limit and the heat transfer coefficient by changing the dynamics of the boiling process (i.e., bubble departure diameter, growth time and frequency, and nucleation site density). This is presumably due to a reduction of the nucleation cavity size. The thin chromium coating covers the uncoated surface conformally, cluttering small cavities and crevices that may serve as nucleation sites. Interestingly, while the uncoated zircoloy-4 and FeCrAl surfaces have different surface finish and boiling behavior, after these surfaces are coated with a 0.3 μm thick chromium layer, their surface properties are equivalent, and their boiling behavior is practically identical. This result has additional implications, as it suggests that the effusivity of the materials plays a minor role compared to the surface finish. In summary, this work confirms that, in flow boiling conditions, the effect of wettability or effusivity may be less important compared to pool boiling conditions. Instead, the boiling process may be determined by the size distribution of the nucleation sites, which, in turn, depends on the surface finish at the micron and submicron scale.

Declaration of Competing Interest

The authors declare that they have no known competing financial interests or personal relationships that could have appeared to influence the work reported in this paper.

CRediT authorship contribution statement

J. H. Seong: Conceptualization, Methodology, Validation, Formal analysis, Investigation, Writing – original draft, Visualization. **C. Wang:** Methodology, Investigation, Writing – review & editing. **B. Phillips:** Methodology, Investigation, Writing – review & editing, Supervision. **M. Bucci:** Conceptualization, Methodology, Writing – review & editing, Supervision, Project administration, Funding acquisition.

Acknowledgements

We acknowledge Profs. Jacopo Buongiorno and Emilio Baglietto for insightful comments on this work. We acknowledge the funding support of the US Nuclear Regulatory Commission (NRC) and the Department of Energy through the Consortium for the Advanced Simulation of Light Water Reactors (CASL).

References

[1] J. Carmack, F. Goldner, S. M. Bragg-Sitton, L. L. Snead, Overview of the U.S. DOE accident tolerant fuel development program, Top Fuel 2013, INL/CON-13-29288 (2013).

[2] B. A. Pint, K. A. Terrani, M. P. Brady, T. Cheng, J. R. Keiser, High-temperature oxidation of fuel cladding candidate materials in steam hydrogen environments, J. Nucl. Mater. 440 (1-3) (2013) 420-427.

[3] J. D. Stempien, D. M. Carpenter, G. Kohse, M. S. Kazimi, Characteristics of composite silicon carbide fuel cladding after irradiation under simulated PWR conditions, Nucl. Technol. 183 (2013) 13-29.

[4] H. G. Kim, I. H. Kim, J. Y. Park, Y. H. Koo, Application of coating technology on Zirconium-based alloy to decrease high-temperature oxidation. Zirconium in the Nuclear Industry: 17th International Symposium, STP (2014) 1543.

[5] H. G. Kim, J. H. Yang, W. J. Kim, Y. H. Koo, Development status of accident-tolerant fuel for light water reactors in Korea, Nucl. Eng. Technol. 48 (2016) 1-15.

[6] B. Chang, Y. J. Kim, P. Chou, Improving accident tolerance of nuclear fuel with coated Mo-alloy cladding, Nucl. Eng. Technol. 48(1) (2016) 16.

[7] M. Sevecek, A. Gurgen, A. Seshadri, Y. Che, M. Wagih, B. Phillips, V. Champagne, K. Shirvan, Development of Cr cold spray-coated fuel cladding with enhanced accident tolerance, Nuc. Eng. Tech. 50 (2018) 229-236.

[8] R. V. Umretiya, S. Vargas, D. Galeano, R. Mohammadi, C. E. Castano, J. V. Rojas, Effect of surface characteristics and environmental aging on wetting of Cr-coated Zircaloy-4 accident tolerant fuel cladding material, J. Nucl. Mat. 535 (2020) 152163.

[9] D. H. Kam, J. H. Lee, T. Lee, Y. H. Jeong, Critical heat flux for SiC-and Cr-coated plates under atmospheric condition, Ann. Nucl. Energy 76 (2015) 335-342.

[10] H. H. Son, G. H Seo, U. Jeong, D. Y. Shin, S. J. Kim, Capillary wicking effect of a Cr-sputtered superhydrophilic surface on enhancement of pool boiling critical heat flux, Int. J. Heat Mass Transf. 113 (2017) 115-128.

[11] H. H. Son, Y. S. Cho, S. J. Kim, Experimental study of saturated pool boiling heat transfer with FeCrAl- and Cr-layered vertical tubes under atmospheric pressure, Int. J. Heat Mass Transf. 128 (2019) 418-430.

[12] N. Kim, H. H. Son, S. J. Kim, Oxidation effect on pool boiling critical heat flux enhancement

of Cr-coated surface for accident-tolerant fuel cladding application, Int. J. Heat Mass Transf. 144 (2019) 118655.
[13] H. Jo, H. Yeom, E. Gutierrez, K. Sridharan, M. Corradini, Evaluation of critical heat flux of ATF candidate coating materials in pool boiling, Nucl. Eng. Des. 354 (2019) 110166.
[14] H. H. Son, S. J. Kim, Role of receding capillary flow correlating nano/micro scale surface roughness and wettability with pool boiling critical heat flux, Int. J. Heat Mass Transf. 138 (2019) 985–1001.
[15] H. H. Son, N. Kim, S. J. Kim, Nano/microscale roughness control of accident-tolerant Cr- and CrAl-coated surfaces to enhance critical heat flux, Appl. Them. Eng. 167 (2020) 11478.
[16] D. Lee, B. Elward, P. Brooks, R. Umretiya, J. Rojas, M. Bucci, R. B. Rebak, M. Anderson, Enhanced flow boiling heat transfer on chromium coated Zircaloy-4 using cold spray technique for Accident Tolerant Fuel (ATF) materials, Appl. Therm. Eng. 185 (2020) 116347.
[17] J. H. Seong, C. Wang, B. Phillips, M. Bucci, Separate effect of oxidation on the subcooled flow boiling performance of Zircaloy-4 at atmospheric pressure, Int. J. Heat Mass Transf. 188 (2022) 122620.
[18] A. Richenderfer, A. Kossolapov, J. H. Seong, G. Saccone, E. Demarly, R. Kommajosyula, E. Baglietto, J. Buongiorno, M. Bucci, Investigation of subcooled flow boiling and CHF using high-resolution diagnostics, Exp. Therm. Fluid Sci. 99 (2018) 35-58.
[19] J. Buongiorno, Can corrosion and CRUD actually improve safety margins in LWRs? Ann. Nucl. Energy 63 (2014) 9-21.
[20] M. Carne, D. H. Charlesworth, Thermal conduction effects on the critical heat flux in pool boiling, Chem. Engng. Prog. Symp. 62 (1966) 24-34.
[21] F. Tachibana, M. Akiyama, H. Kawamura, Non-hydrodynamic aspects of pool boiling burnout, J. Nucl. Eng. Technol. 4 (3) (1967) 121-130.
[22] U. Magrini, E. Nannei, On the influence of the thickness and thermal properties of heating walls on the heat transfer coefficients in nucleate pool boiling, J. Heat Transf. 97 (2) (1975) 173-178.
[23] G. Guglielmini, E. Nannei, On the effect of heating wall thickness on pool boiling burnout, Int. J. Heat Mass Transf. 19 (1976) 1073-1075.
[24] A. Bar-Cohen, A. McNeil, Parametric effects on pool boiling critical heat flux in highly wetting liquids, in: Proceedings of Engineering Foundation Conference on Pool and Externernal

Flow Boiling (1992) 171-176.
[25] I. Golobic, A. E. Bergles, Effects of heater-side factors on the saturated pool boiling critical heat flux, Exp. Therm. Fluid Sci. 15 (1997) 43-51.
[26] M. Arik, A. Bar-Cohen, Effusivity-based correlation of surface property effects in pool boiling CHF of dielectric liquids, Int. J. Heat Mass Transf. 26 (2003), 3755-3764.
[27] I. I. Gogonin, Influence of the thickness of a wall and of its thermophysical characteristics on the critical heat flux in boiling, J. Eng. Phys. Thermophys. 82 (6) (2009) 1175-1183.
[28] P. A. Raghupathi, S. G. Kandlikar, Effect of thermophysical properties of the heater substrate on critical heat flux in pool boiling, J. Heat Transf. 139 (11) (2017) 111502 1-7.
[29] M.V.H. Del Valle, An experimental study of critical heat flux in subcooled flow boiling at low pressure including the effect of wall thickness, in: Proceedings of ASME-JSME Thermal Engineering Joint Conference (1983) 143-150.
[30] J. H. Seong, Investigation of separate effects of surface condition on subcooled flow boiling heat transfer, PhD thesis, Massachusetts Institute of Technology, Cambridge, MA (2021) 58-67.
[31] T. Falk, et al., U-Net: deep learning for cell counting, detection, and morphometry, Nature Methods 16 (1) (2019) 67-70.
[32] J. H. Seong, M. S. Song, D. Nunez, A. Manera, E. S. Kim, Velocity refinement of PIV using global optical flow, Exp. Fluids 60 (174) (2019).
[33] M. Bucci, J. Buongiorno, M. Bucci, The not-so-subtle flaws of the force balance approach to predict the departure of bubbles in boiling heat transfer, Physics of Fluids, 33(1) (2021).
[34] V. P. Carey, Liquid-vapor phase-change phenomena: an introduction to the thermophysics of vaporization and condensation processes in heat transfer equipment. CRC Press (2020).
[35] T. Mazzocco, W. Ambrosini, R. Kommajosyula, E. Baglietto, A reassessed model for mechanistic prediction of bubble departure and lift off diameters, Int. J. Heat Mass Transf. 117 (2018) 119-124.
[36] G.Y. Su, C. Wang, L. Zhang, J.H. Seong, R. Kommajosyula, B. Phillips, M. Bucci, Investigation of flow boiling heat transfer and boiling crisis on a rough surface using infrared thermometry. Int. J. Heat Mass Transf. 160 (2020) 120134.
[37] Y. Y. Hsu, On the size range of active nucleation cavities on a heating surface, J. Heat Transf. 84 (3) (1962) 207-213.

Appendix A.

Fig. 7 and Fig. 8 show boiling curves and bubble parameters for the second runs, respectively. The repeated tests corroborate the results discussed in Section 4.

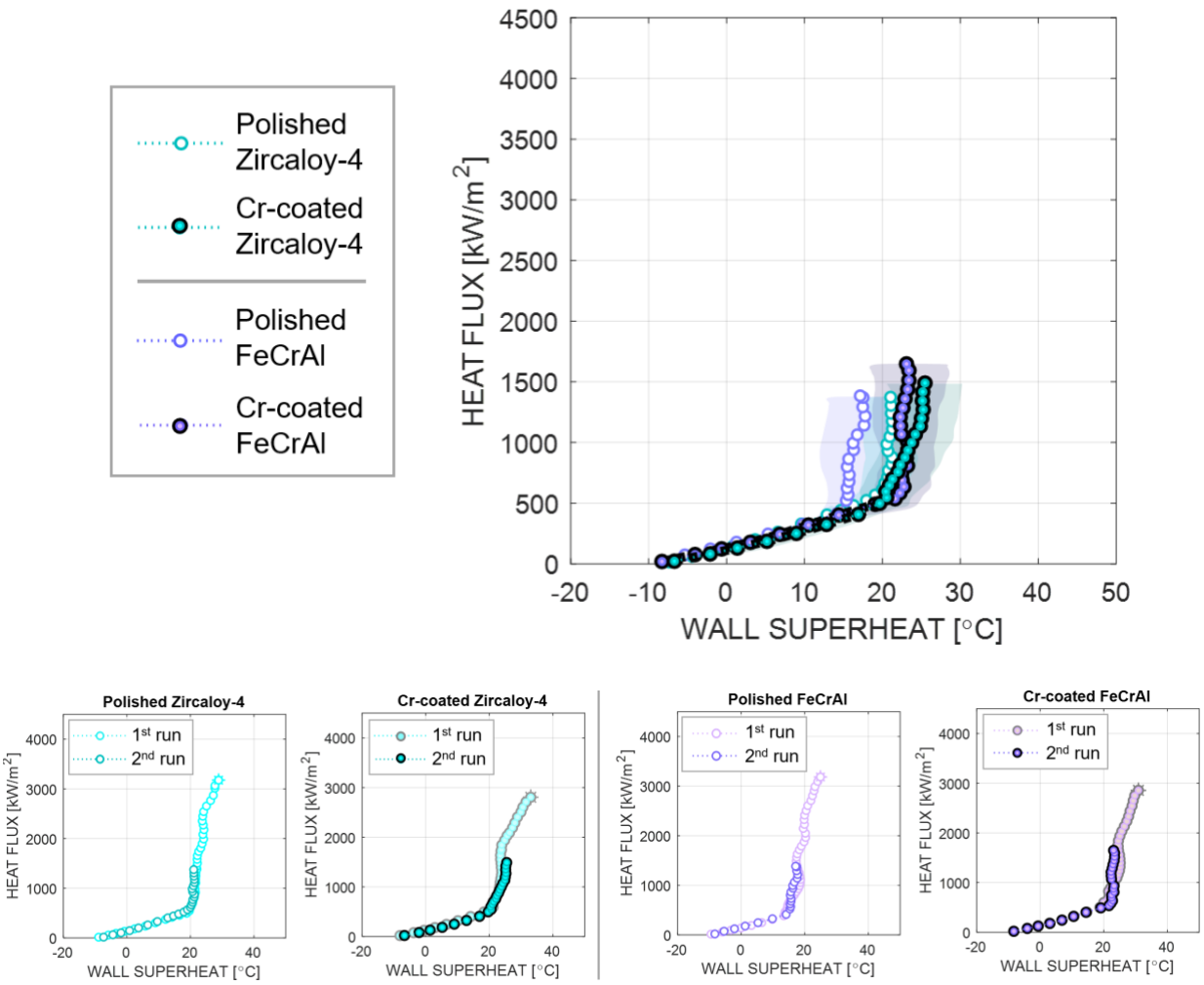

Fig. 7. Boiling curves of the second runs.

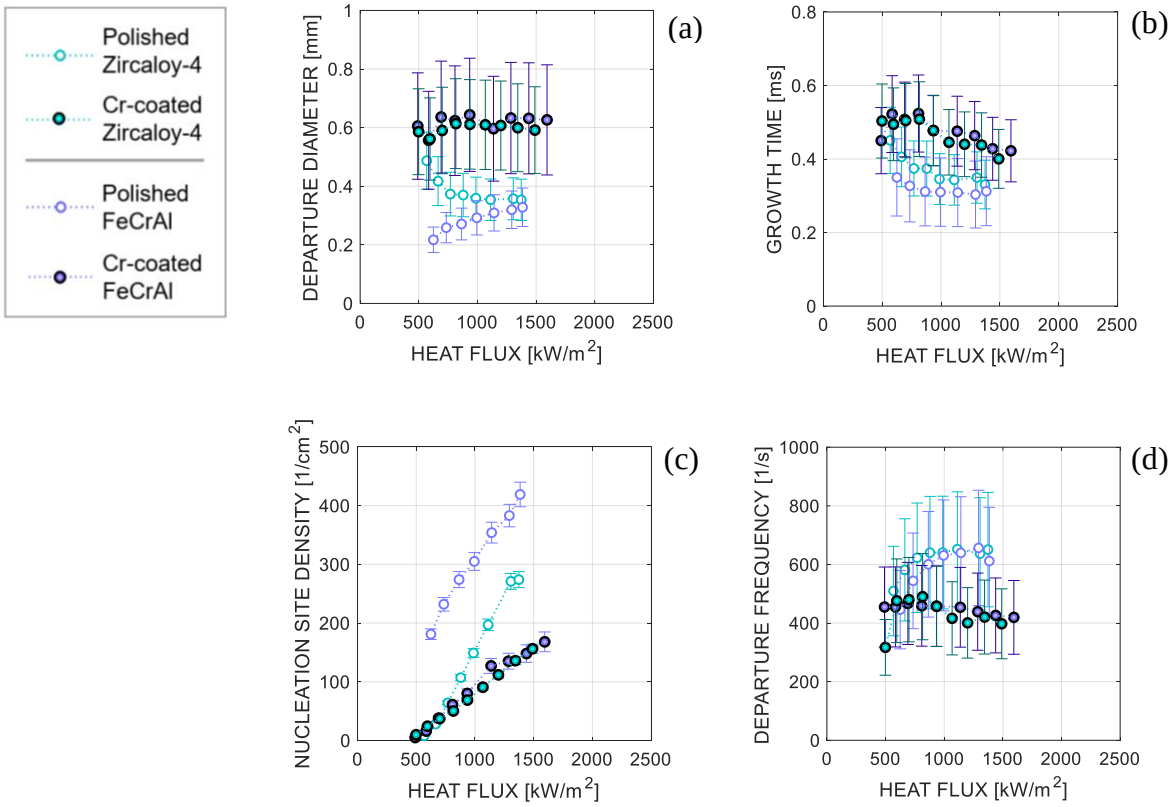

Fig. 8. Measured departure diameter (a), growth time (b), nucleation site density (c), and bubble departure frequency (d), at several heat fluxes, for the second runs.

Appendix B. Thermal effusivity and diffusivity of materials

Fig. 9 show the thermal effusivity (left) and diffusivity (right) of zircaloy-4, FeCrAl, other materials of interest for the nuclear industry (e.g., Inconel and stainless steel 316), and other materials often used for boiling heat transfer investigations (e.g., copper, aluminum, sapphire and silicon).

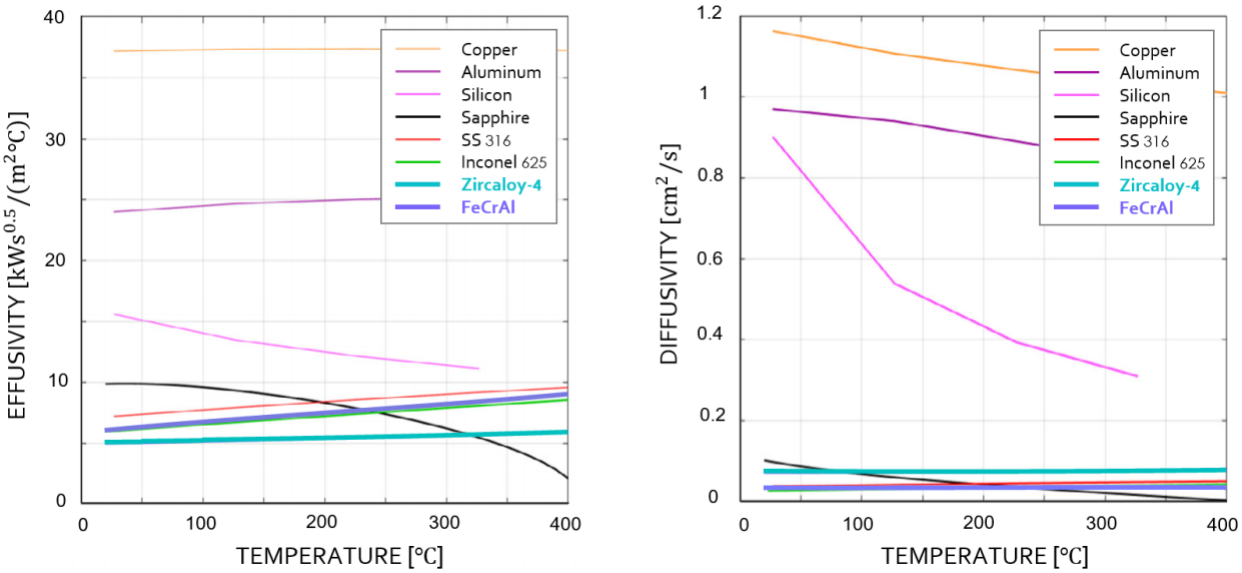

Fig. 9. Thermal effusivity and thermal diffusivity of Zircaloy-4, FeCrAl, and other materials as function of temperature.